JOURNAL OF MATERIALS SCIENCE 26 (1991) 4033–4047

Polypropylene/ethylene-co-propylene blends: influence of molecular structure of EPR and composition on phase structure of isothermally crystallized samples

L. D'ORAZIO, C. MANCARELLA, E. MARTUSCELLI, G. STICOTTI
Istituto di Ricerche su Tecnologia dei Polimeri e Reologia del C.N.R., Via Toiano, 6 80072 Arco Felice, Napoli, Italy

The structure of phases and interphases in samples crystallized under controlled undercoolings, of isotactic polypropylene/ethylene-co-propylene copolymers (iPP/EPR blends) was examined using optical and electron microscopy and small-angle X-ray scattering and differential scanning calorimetry. The study was undertaken to establish the influence of molecular structure of the EPR copolymers and blend composition on the phase structure developed in samples isothermally crystallized at relatively low undercoolings. Optical and electron microscopy revealed that the molecular structure and composition of the EPR phase play a predominant role in determining the mode and state of dispersion of the minor rubber component. It was also found that the crystallization process of iPP from its blends was influenced by the presence of the EPR phase with no regular dependence on its molecular structure and composition. For a given crystallization temperature, a decrease in thickness of the crystalline lamellae, L_c, and an increase in the amorphous interlamellar layer, L_a were observed. The L_c and L_a values were found to be strictly related to the blend composition; L_c decreasing and L_a increasing with increasing EPR content in the blend.

1. Introduction

The results of an investigation of the influence of the average molecular mass and molecular weight distribution (MWD) and of the propylene content (C_3) (wt/wt) of ethylene-co-propylene copolymers (EPR) on melt rheology, mode and state of dispersion of the minor component in the melt, as well as in the solid state, and on the impact properties of injection-moulded samples of iPP based blends, were reported in a previous paper [1]. From such studies aimed at correlating molecular structure and composition of EPR with melt rheological behaviour, size of rubbery particles and impact resistance of the blend system, it was found that the dispersion coarseness of the minor component increases with decreasing zero shear viscosity of the blends, according to the results already obtained while studying a different incompatible blend system made from PA6 and ethylene-co-vinyl-acetate copolymers [2].

The size and size distribution of EPR domains were determined by the value of phase viscosity ratio, μ, defined as the ratio between the zero shear viscosity of the dispersed phase and the zero shear viscosity of the matrix, irrespective of C_3 content along the EPR chain. The trend of the number-average particle diameter, $\bar{D}_n$, versus $\log \mu$ showed that $\bar{D}_n$ decreases with decreasing $\log \mu$, in agreement with expectations on the basis of the Taylor–Tomotika theory, according to which, the particle size versus $\log \mu$ function shows a minimum in the vicinity of $\mu = 1$ [3, 5]. The range of particle size effective for iPP toughening was found to be dependent on test temperature; for temperatures higher than the T_g of EPR and close to T_g of iPP such a range is narrower than that effective at room temperature (T_g is the glass transition temperature).

In the present paper, the results of an investigation of the influence of molecular mass and MWD and of C_3 content (wt/wt) of EPR copolymers, and of the overall composition on the phase morphology and structure developed in iPP/EPR samples isothermally crystallized at relatively low values of undercooling, are reported.

The main aim of the work was to determine how the EPR molecular structure and/or overall blend composition may determine the mode and the state of dispersion of the minor component and its location in inter- and/or intraspherulitic regions of iPP, the iPP spherulites texture and their crystallinity and structure.

Finally, the combined effect of undercooling and EPR molecular structure and composition on the kinetic and thermodynamic parameters related to the crystallization process of the iPP phase, was also investigated.

0022–2461/91 $03.00 + .12

TABLE I Molecular characteristics, glass transition, T_g, and observed melting temperature, T'_m, of neat isotactic polypropylene (iPP) and ethylene/propylene copolymers (EPR)

Sample	M.F.I. (g/10 min)	Mooney viscosity,[a] ML(1 + 4)	C_3 content (% wt/wt)	M_w/M_n	T_g (°C)	T'_m (°C)
iPP	1.75			7.4	− 10	166
EPR1		25	27	3.5	− 41	45
EPR2		67	28	3.5	− 40	48
EPR3		80	43	5.0	− 45	–
EPR4		55	58	3.5	–	–

[a] Measured at 120 °C.

2. Experimental procedure

2.1. Materials

The polymers used in this study were an isotactic polypropylene (iPP) (Moplen S30G) and four commercial ethylene-propylene random copolymers (EPR; EPR1, EPR2, EPR3, EPR4). The molecular characteristics of these polymers are summarized in Table I.

2.2. Blending and sample preparation

The iPP and the EPR copolymers were mixed in a Werner mixer at 230 °C with a blending time of 3 min. Blends with composition iPP/EPR 90/10 (wt/wt) and 80/20 (wt/wt) were prepared. After blending, the materials were injection moulded using an injection press GBF 160/72 at 230 °C with a mould temperature of 60 °C.

2.3. DSC measurements

The apparent melting temperatures, T'_m, and the crystallinity index of the neat iPP, X_c(iPP), and iPP crystallized isothermally at 123, 128, 133, 138 and 145 °C from its blends with EPR copolymers, X_c(blend), were determined by differential scanning calorimetry (DSC, Mettler TA 3000) equipped with a control and programming unit (microprocessor T_c 10) using the following procedure. The samples (about 10–12 mg), heated to 488 K at a rate of 20 K min^{-1} and kept at this temperature for 15 min, were rapidly cooled to the required crystallization temperature, T_c; after complete crystallization, such samples were again heated to 488 K at a rate of 20 K min^{-1}. The observed melting temperature, T'_m, and the apparent enthalpies of melting, ΔH^*, were obtained from the maxima and the area of the melting peaks, respectively. The crystallinity index of the iPP phase and of the overall blends were calculated from

$$X_c(\text{iPP}) = \frac{\Delta H^*(\text{iPP})}{\Delta H^0(\text{iPP})} \quad (1)$$

$$X_c(\text{blend}) = \frac{\Delta H^*(\text{blend})}{\Delta H^0(\text{iPP})} \quad (2)$$

where ΔH^*(iPP) is the apparent enthalpy of fusion per gram of iPP in the blend; ΔH^0(iPP) is the heat of fusion per gram of 100% crystalline iPP (from [6] ΔH^0(iPP) = 209 J g^{-1}), and ΔH^*(blend) is the apparent enthalpy of fusion per gram of blend.

2.4. Radial growth rate measurements

The iPP radial growth rates $G = dR/dt$, (where R is the radius of spherulite, and t the time) were calculated by measuring the spherulite size as a function of time during the isothermal crystallization processes at 123, 133 and 145 °C undergone by thin films, using an optical polarizing Leitz microscope. In order to eliminate the probable effect of the mould walls on concentration and shape of the EPR particles, the thin films were obtained from the central part of a transverse section of the injection-moulded bars according to the following procedure: the materials were squeezed between a microscope slide and a cover glass, heated at 200 °C and kept at this temperature for 10 min to destroy any trace of crystallinity; the temperature was then rapidly lowered to T_c and the material allowed to crystallize isothermally. The photomicrographs were taken on the grown iPP spherulites at appropriate intervals. The radius, R, was measured on the print and G calculated as the slope of the straight lines obtained by plotting R against time.

2.5. Investigation of morphology

The overall morphology developed in samples of plain iPP and iPP/EPR blends isothermally crystallized from the melt at the temperatures of 123, 133 and 145 °C was analysed using optical and scanning electron microscopy. Optical micrographs of thin films, obtained and crystallized according to the procedure reported previously, were taken at crossed and parallel polars using a Leitz polarizing microscope equipped with a Mettler hot stage.

Cryogenic fracture surfaces of parallelepiped-shaped specimens about 2 mm thick, isothermally crystallized in the Mettler hot stage, were observed using a Philips 501 scanning electron microscope after coating with Au–Pd in a sputtering Polaron equipment LTD E S/50.

2.6. Small angle X-ray analysis

Small-angle X-ray scattering (SAXS) studies, performed on samples of the neat iPP and iPP isothermally crystallized from its blends with EPR copolymers at 123, 133, 138 and 145 °C were carried out using a compact Kratky camera equipped with a Braun one-dimensional positional sensitive detector. Ni-filtered CuK_α radiation, generated from a Philips X-ray generator (PW 1730/10) operating at 40 kV

and 30 μA, was used. The raw scattering data were corrected for parasitic scattering, absorption and slit smearing using Glatter's method [7]. The desmeared intensities were then Lorentz-factor corrected [8] by multiplying by s^2 ($s = 2\sin\Theta/\lambda$).

3. Results and discussion

3.1. Apparent melting temperatures and crystallinity

The DSC thermograms of samples of the neat iPP and iPP/EPR blends isothermally crystallized at 123, 128, 133, 138 and 145 °C show a single sharp endothermic peak when heated from the crystallization temperature up to 215 °C; the temperature position of these peaks, T'_m, reported in Table II, is characteristic of the melting of the α crystalline form of iPP. As shown in the table, the values of T'_m of both neat iPP and iPP crystallized from its blends with EPR copolymers increase with increasing T_c, indicating, as expected, that the perfection and thickness of the growing iPP lamella crystal increases with increasing T_c. Furthermore, the T'_m values exhibited, for a given T_c, by the iPP crystallized in the presence of EPR, irrespective of the copolymer content in the blend and its molecular structure and composition, are very close to each other and strictly approach that shown by the neat iPP. Such findings indicate that the melting behaviour of iPP is independent of both blend composition and EPR molecular structure and composition: the perfection of the growing iPP crystals is not influenced by the presence of the EPR rubbery phase, irrespective of its molecular characteristics. Thus, according to Martuscelli [9, 10] iPP and EPR copolymers are confirmed to be incompatible in the molten state.

The crystallinity index of the iPP/EPR blends, X_c(blend), and of the iPP phase, X_c(iPP), are reported in Tables III and IV, respectively, as a function of T_c. Note that:

(i) for a given blend composition both X_c(blend) and X_c(iPP) slightly increase with increasing T_c with no dependence on EPR molecular structure and composition;

(ii) for a given T_c, the X_c(blend) values, decreasing with increasing EPR content, are close to each other, irrespective of EPR molecular structure and composition. Moreover, such X_c(blend) values remain lower than that shown by the neat iPP. In turn, the X_c(iPP) values shown by the iPP phase crystallized in the presence of 10% (wt/wt) and 20% (wt/wt) EPR copolymer are, respectively, about 1.2 and 1.5 times lower than that exhibited by the neat iPP phase with no dependence on EPR molecular structure and composition. Such an observation suggests that the presence of the EPR rubbery phase, irrespective of its molecular characteristics, influences the crystallization process of iPP from its blends with EPR.

TABLE II Observed melting temperatures, T'_m, for plain iPP and iPP crystallized isothermally from its blend with EPR copolymers as a function of crystallization temperature, T_c

Sample		T'_m (°C) at T_c (°C):				
		123	128	133	138	145
iPP 100		162	163	166	169	176
iPP/EPR1	90/10	162	162	165	168	173
iPP/EPR1	80/20	161	163	165	168	174
iPP/EPR2	90/10	161	162	166	169	173
iPP/EPR2	80/20	161	162	165	168	174
iPP/EPR3	90/10	161	162	166	168	174
iPP/EPR3	80/20	161	162	165	168	174
iPP/EPR4	80/20	163	163	164	167	174

TABLE III Overall blend crystallinity, X_c(blend), as a function of crystallization temperature, T_c

Sample		X_c(blend) (%) at T_c (°C):				
		123	128	133	138	145
iPP 100		43	44	43	45	46
iPP/EPR1	90/10	39	40	40	41	42
iPP/EPR1	80/20	35	36	36	37	38
iPP/EPR2	90/10	38	38	39	41	42
iPP/EPR2	80/20	33	33	35	37	37
iPP/EPR3	90/10	36	40	41	42	42
iPP/EPR3	80/20	36	34	36	37	38
iPP/EPR4	80/20	35	35	36	38	39

TABLE IV Crystallinity index of iPP phase, X_c(iPP), as a function of crystallization temperature, T_c

Sample		X_c(iPP) (%) at T_c (°C):				
		123	128	133	138	145
iPP 100		43	44	43	45	46
iPP/EPR1	90/10	35	36	36	37	38
iPP/EPR1	80/20	28	29	29	29	30
iPP/EPR2	90/10	34	35	35	36	38
iPP/EPR2	80/20	26	27	28	29	30
iPP/EPR3	90/10	33	36	37	38	38
iPP/EPR3	80/20	29	27	29	29	30
iPP/EPR4	80/20	28	28	29	30	31

3.2. Radial growth rate of iPP spherulites

Plots of the radius of iPP spherulites against time for all crystallization temperatures and blend compositions investigated, give straight lines indicating that, irrespective of EPR molecular structure and composition, the concentration of iPP crystallizable molecules at the growth front is constant during the crystallization process. Plots of radial growth rate, G, of iPP spherulites as a function of crystallization temperature, T_c, for all the blend compositions investigated, are shown in Fig. 1. From the trend of the curves it emerges that the addition of EPR to iPP produces, at a given T_c, no change in G. This finding, in agreement with the melting behaviour of blends previously discussed, indicates that no favourable specific interactions between the two components exist, irrespective of copolymer molecular structure and composition. Thus it seems reasonable to suppose that in the iPP/EPR melt the EPR component is present with its own domains. Consequently, for iPP/EPR blends the

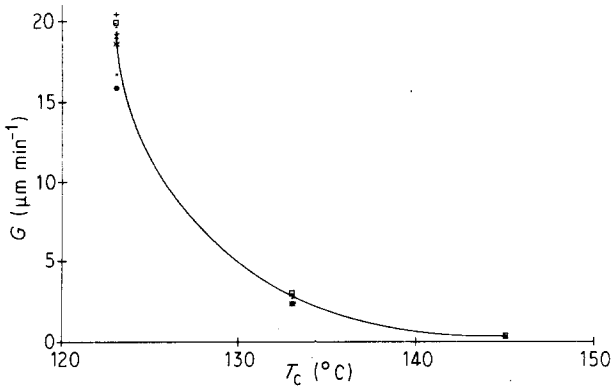

Figure 1 Radial growth rate, G, of iPP spherulites as a function of crystallization temperature.

iPP spherulites grow from a non-homogeneous melt characterized by the presence of domains of almost neat rubber dispersed in a melt matrix of almost neat iPP.

3.3. Mode and state of dispersion of the minor component and spherulite texture

Optical micrographs, taken at crossed and parallel polars, of thin films of the neat iPP and iPP/EPR blends isothermally crystallized at 123, 133 and 145 °C, are shown in Figs 2–9. As expected on the basis of the results already obtained by Martuscelli while studying the isothermal crystallization process of iPP based blends [9, 10], the EPR minor component segregates mainly in spherical-shaped domains distributed in the intraspherulitic and interspherulitic regions. Moreover, it can be observed that the addition of EPR copolymers may affect the shape, size and regularity of iPP spherulites.

It should also be noted that the dispersion coarseness of the rubbery phase and the structural change undergone by the iPP spherulites were strongly determined, in addition to the overall blend composition and the crystallization temperature, by the EPR molecular structure. Moreover, for both neat iPP and iPP crystallized from its blends with EPR copolymers, at the intermediate crystallization temperature investigated (133 °C), large amorphous interspherulitic contact regions were observed and the thickness of such regions became wider with increasing T_c. This result suggests that for high undercoolings (T_c = 123 °C) the amorphous material is predominantly located in the intraspherulitic regions, whereas for intermediate and low undercoolings (T_c = 133 and 145 °C, respectively)

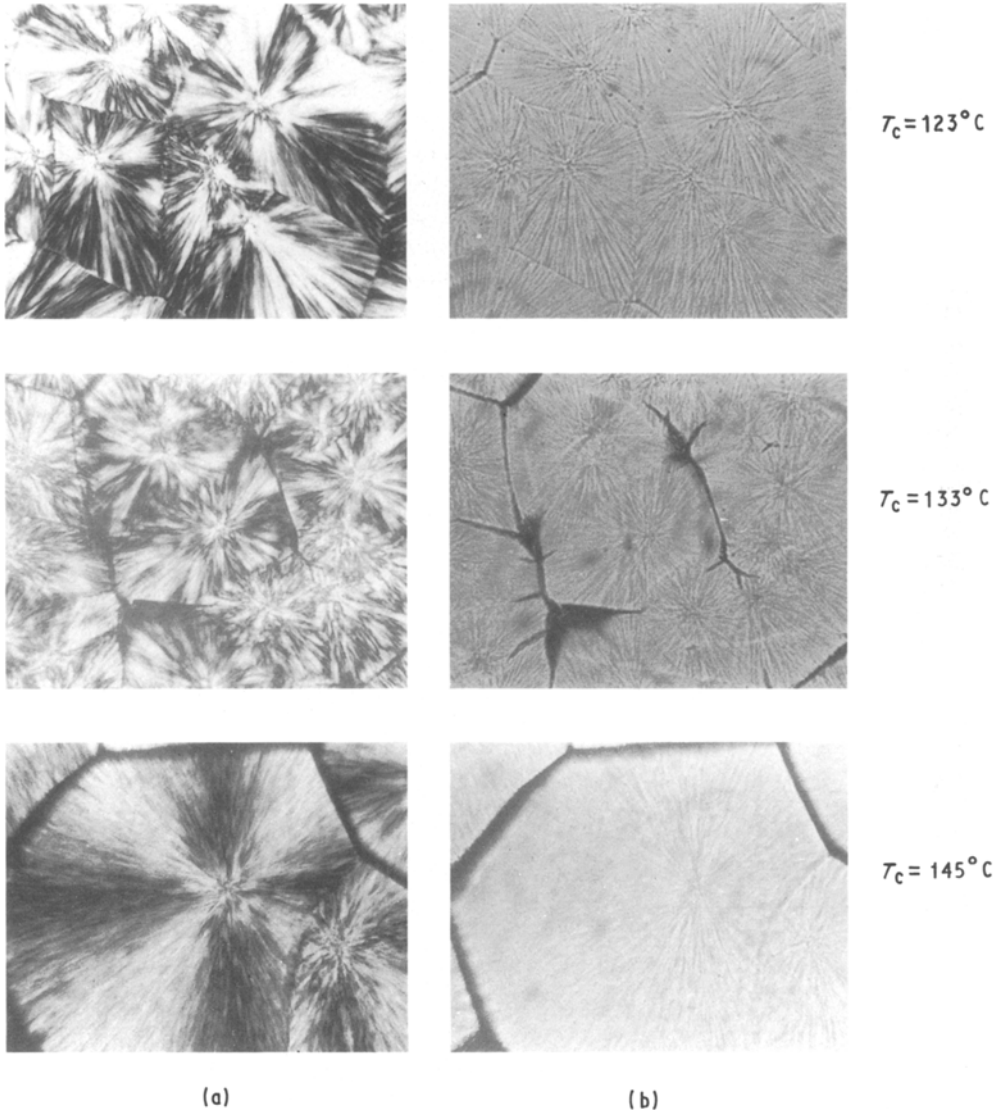

Figure 2 Optical micrographs taken at (a) crossed and (b) parallel polars of the neat iPP. × 25.2.

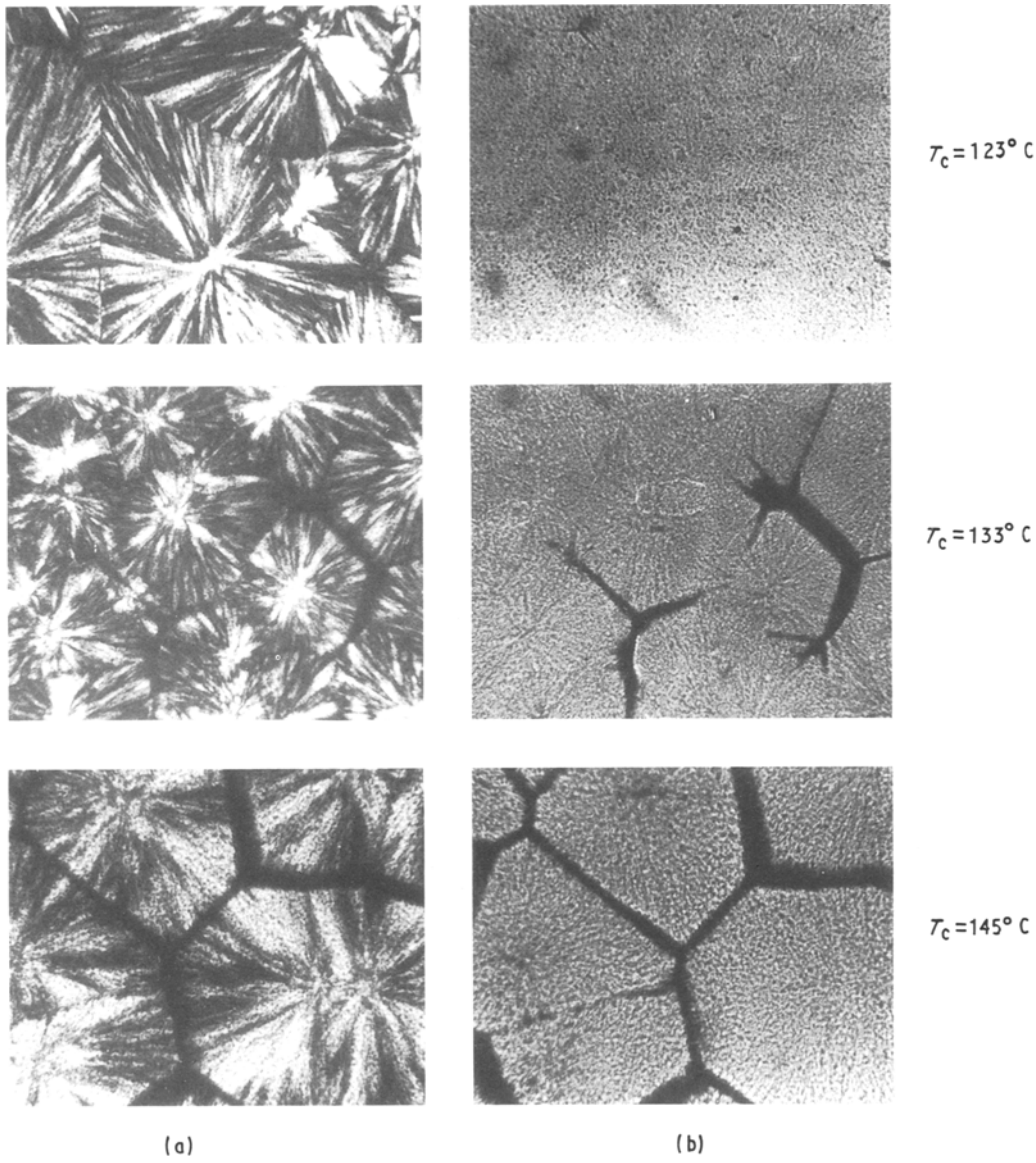

Figure 3 Optical micrographs taken at (a) crossed and (b) parallel polars of iPP/EPR1 (90/10). × 25.2.

it tends more and more to be rejected into interspherulitic contact regions.

3.3.1. Effect of the overall blend composition

A study of the effect of the composition on mode and state of dispersion of the minor component developed in the iPP/EPR system isothermally crystallized has been reported by Martuscelli [9]. With increasing rubber content, coalescence and occlusion of the EPR spherical-shaped domains were found to be the most relevant factors. The range of EPR particle size generated in the iPP/EPR blends investigated in the present paper, isothermally crystallized at 133 and 145 °C, are reported in Table V which shows that no systematic dependence of the EPR particle size on the overall blend composition can be observed. In fact, with increasing EPR content, the range of particle size, developed in the blends containing the EPR1 and EPR2 copolymers widens, whereas the range of particle size shown by the blend containing the EPR3 copolymer remains constant with composition.

On the other hand, systematic dependence of the neatness and regularity of iPP spherulites crystallized in the presence of EPR phase on the overall blend composition can be observed. As shown by comparing Figs 3 and 6 and Figs 5 and 8, the neatness and regularity of iPP spherulites were found to decrease with increasing EPR content. By comparing Figs 4 and 7 and Figs 5 and 8 it also emerges that the thickness of the amorphous interspherulitic contact regions, for a given T_c, and especially at lower ΔT, tends to increase with increasing EPR content. This indicates that the amount of amorphous material which, for a given T_c, is rejected into the interspherulitic regions increases with increasing rubber content.

3.3.2. Effect of crystallization temperature

The mode and state of dispersion of the EPR dispersed phase, for a given blend composition, was found to be independent of crystallization temperature. The range of the EPR particle size is found to be constant

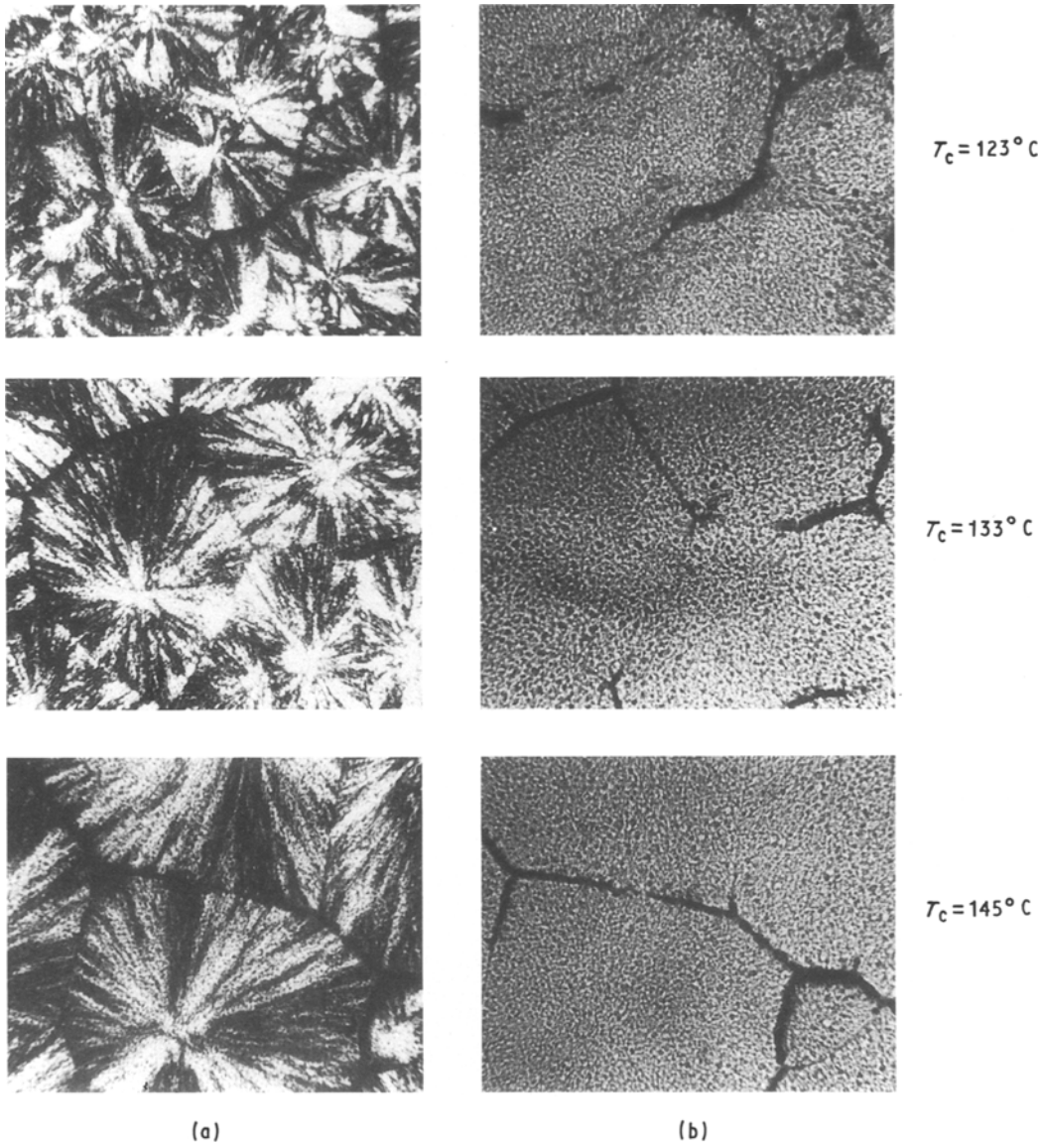

Figure 4 Optical micrographs taken at (a) crossed and (b) parallel polars of iPP/EPR2 (90/10). × 25.2.

with T_c (see Table V). Moreover, as expected, for all investigated samples the largest spherulites were obtained at lower undercoolings (see Figs 2–9). This again indicates that for a given blend composition, the amount of amorphous material rejected in the interspherulitic contact regions, increases with increasing T_c.

3.3.3. Effect of EPR molecular mass

The molecular mass of the EPR component seems to play a very important role in determining the mode of dispersion of the rubbery component. By comparing Figs 3 and 4 and Figs 6 and 7 it emerges that, for a given blend composition, for all explored T_c, the sample containing EPR1 seems to be characterized by the presence of domains with a finer dispersion than that containing EPR2. SEM investigation performed on cryogenic fracture surfaces of isothermally crystallized bars shows, in fact, that irrespective of blend composition, the dimensions of EPR1 spherical-shaped domains are about half that shown by the EPR2 minor component (see Table V). This finding indicates that the dispersion coarseness of such EPR copolymers tends to increase with increasing melt viscosity; i.e. with increasing phase viscosity ratio defined as $\mu = \mu_a/\mu_c$ where μ_a is the zero shear viscosity of the dispersed phase and μ_c that of matrix. This finding is in agreement with the results obtained by us while studying injection-moulded samples of the same iPP/EPR blends [1]. Furthermore, it can be observed that with increasing EPR molecular mass (refer to the EPR3 sample in Table I) the copolymer dispersion coarseness increases (see Table V and Figs 5 and 8). This finding and the highest value presumably assumed by the phase viscosity ratio, μ, for iPP/EPR3 blend seems to support that the range of particle size shown by such EPR dispersed phases is mainly determined by μ. It should be noted simultaneously that the EPR4 copolymer, even though it has a molecular mass higher than that of the EPR1 copolymer (see Table I), segregates in domains with a dispersion considerably finer than that developed in the sample containing the EPR1 phase (see Table V and compare Figs 9 and 6). The trend of the number-average diameter, $\bar{D}$, of the

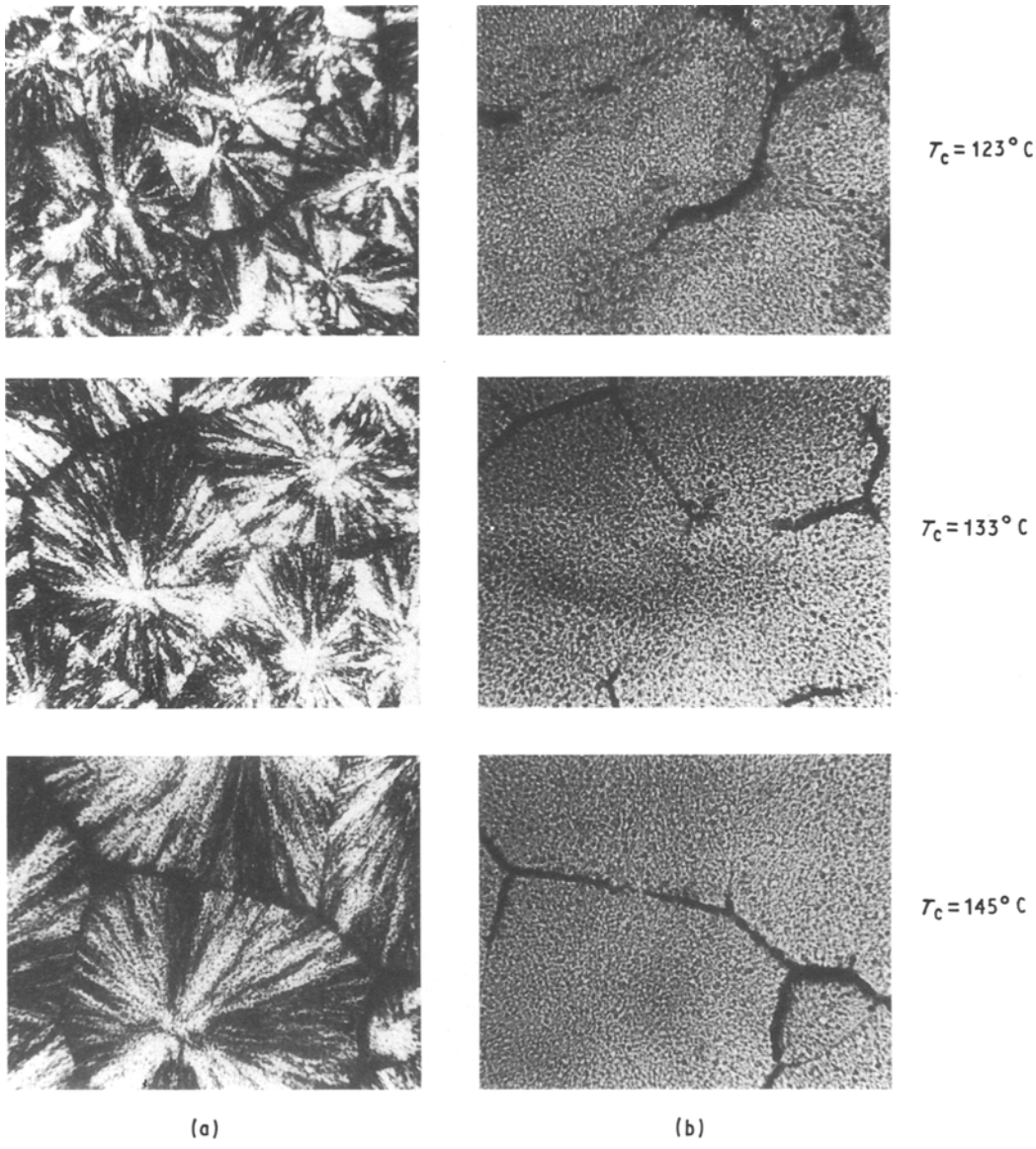

Figure 5 Optical micrographs taken at (a) crossed and (b) parallel polars of iPP/EPR3 (90/10). × 25.2.

EPR particles versus the EPR Mooney viscosity confirms, in fact, that except for the EPR4 sample, D decreases with decreasing melt viscosity of the copolymer; i.e. with decreasing phase viscosity ratio (see Fig. 10). The finding that the sample containing the EPR4 copolymer, irrespective of its molecular mass, shows the finest dispersion, is presumably to be ascribed to the noticeably higher EPR4 propylene content (see Table I), which could promote affinity with the iPP matrix. It cannot be excluded, in fact, that iPP-type blocks are present along the copolymer chains.

Thus the above findings indicated that up to a C_3 content of 43% (wt/wt) the dominant role in determining EPR particle size is played by the copolymer molecular mass.

The EPR molecular mass also seems to play an important role in affecting the neatness and regularity of iPP spherulites and the thickness of the amorphous interspherulitic contact regions. In fact, as shown by comparing Figs 6–8, the iPP spherulite texture appears less neat and regular with increasing EPR molecular mass; i.e. with decreasing μ. Consequently, the amount of amorphous material that for a given T_c, is rejected into interspherulitic contact regions, increases with decreasing EPR molecular mass (compare Figs 3c and 5c and Figs 7c and 8c); i.e. with increasing μ.

3.3.4. Effect of the EPR propylene content

The propylene content (C_3) along the EPR chain also seems to be a critical parameter in determining the mode of dispersion of the rubbery component. By comparing Fig. 9 with Figs 6–8 it emerges that for all explored T_c, the samples containing EPR4 seem to be characterized by the presence of domains with the finest dispersion. SEM investigation shows, in fact, that the EPR4 particles are the smallest in the size being contained in the range 0.3–1 μm (see Table V).

This finding indicates that the lowest dispersion coarseness of the rubbery component is associated with the highest C_3 content along the copolymer chain (58% wt/wt). It is likely that a noticeable reduction in the interfacial tension, induced by the high C_3 content,

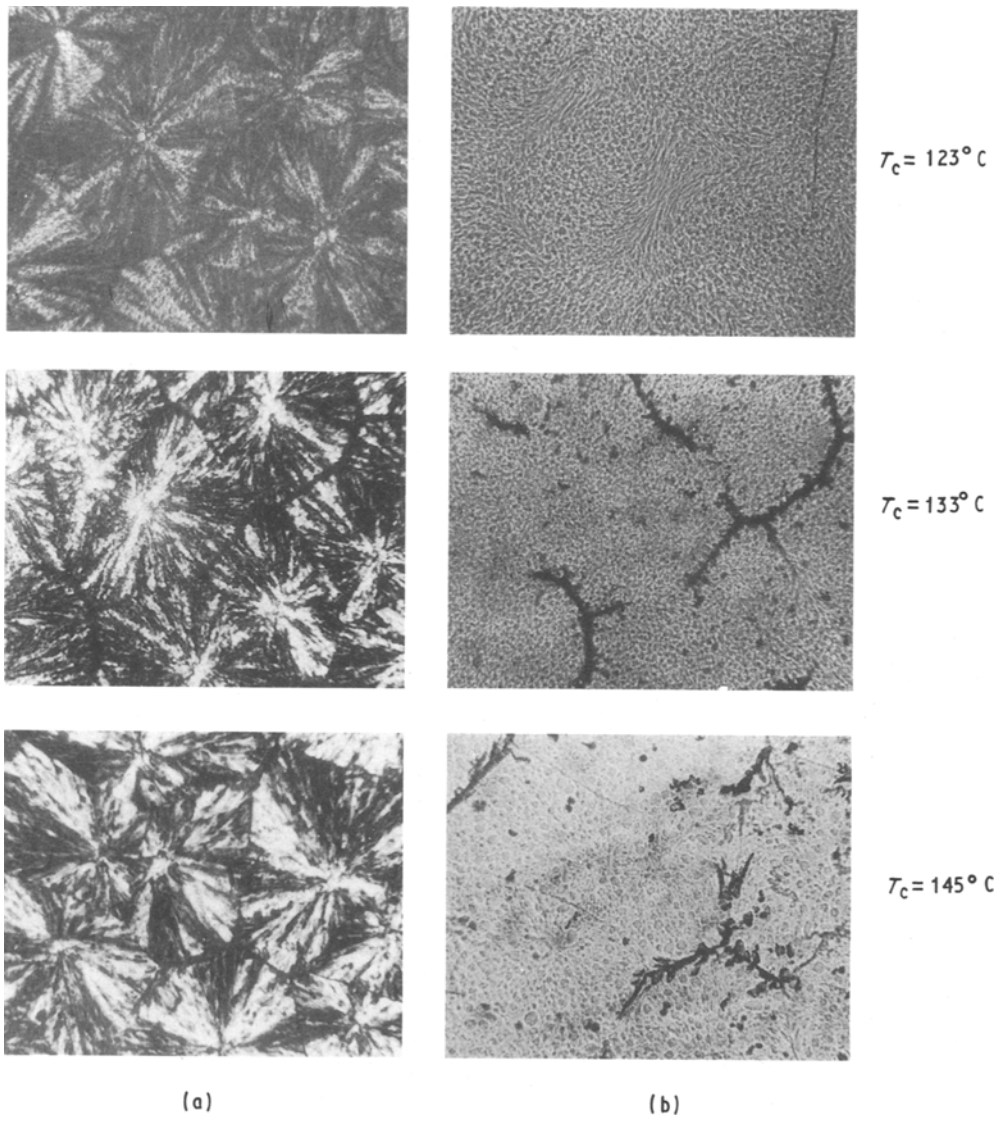

Figure 6 Optical micrographs taken at (a) crossed and (b) parallel polars of iPP/EPR1 (80/20). × 25.2.

is responsible for the very fine dispersion achieved. It should be pointed out that no systematic decrease in particle size with increasing C_3 content can be observed. The sample containing EPR3 shows, in fact, comparatively the coarsest dispersion (compare Fig. 8 with Figs 6, 7 and 9); its particle size ranges between 2 and 4 μm (see Table V). The trend of the number-average diameter of EPR particles versus the EPR propylene content shows, in fact, that the EPR size increases with increasing C_3 content along the copolymer chain up to 43% (wt/wt); whereas with a further increase in C_3, a drop in the EPR particle size is observed (see Fig. 11). This result could be explained by supposing that the higher C_3 content EPR copolymer contains iPP blocks which promote a longer affinity with the iPP matrix molecules.

Note, however, that with increasing C_3 content, no coalescence phenomenon is undergone by domains of the dispersed phase with increasing EPR content; compare the range of particle size shown by the blends containing EPR1 and EPR2 copolymers with that shown by the blends containing EPR3 copolymer. Such a finding indicates that by increasing the C_3 content along the copolymer chain the particles size of the dispersed phase become independent of the overall blend composition.

As shown by comparing Figs 7–9, the iPP spherulite texture seems to be independent of C_3 content along the EPR chain for high and intermediate undercoolings, whereas for low undercoolings the neatness and regularity of the iPP spherulites seem to increase with increasing propylene content along the EPR chain. Moreover, at high T_c, the thickness of the amorphous interspherulitic contact regions tends to increase with decreasing C_3 content along the EPR chain (compare Figs 7–9).

3.4. Superreticular parameters of iPP

Typical Lorentz corrected desmeared patterns for the neat iPP and iPP/EPR blends are shown in Fig. 12. As shown, the desmeared SAXS profiles of both neat iPP and iPP crystallized in the presence of EPR copolymers exhibit well defined maxima. By applying Bragg's law, the long period L, calculated from the peak position, was obtained for all investigated samples as a function of T_c. Assuming a two-phase model

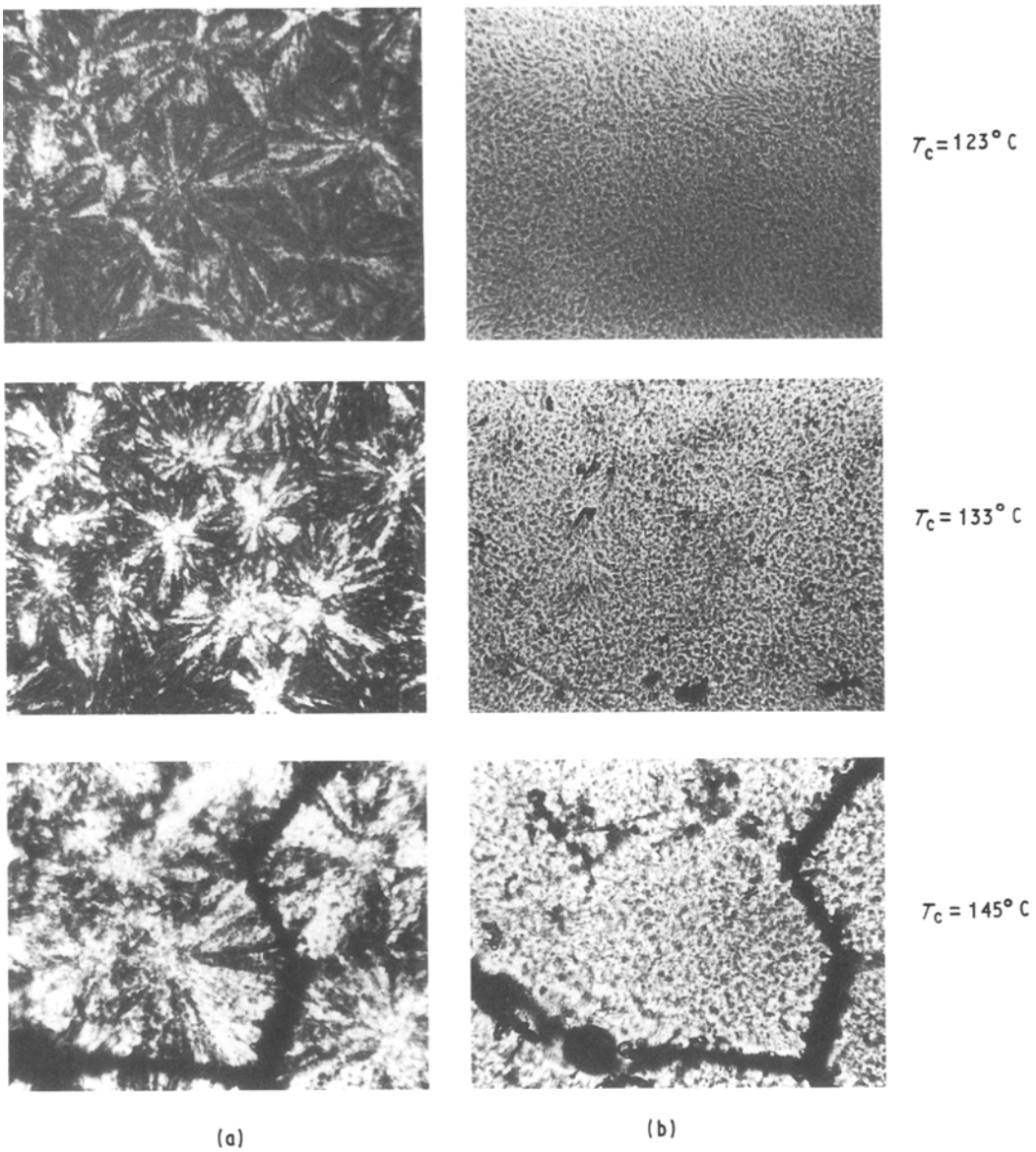

Figure 7 Optical micrographs taken at (a) crossed and (b) parallel polars of iPP/EPR2 (80/20). × 25.2.

for the iPP spherulite fibrillae, consisting of alternating parallel crystalline lamellae and amorphous layers, from the L values, the crystalline lamellar thickness, L_c, was calculated using

$$L_c = \frac{X_c L}{(\rho_c/\rho_a)(1 - X_c(\text{iPP})) + X_c(\text{iPP})} \quad (3)$$

where X_c(iPP) is the DSC crystallinity index of the iPP phase, ρ_c and ρ_a are the densities of the crystalline and amorphous iPP phase, respectively. Subtracting the values of L_c obtained from the L values the average thickness of the amorphous interlamellar layers, L_a, was obtained.

In this calculation, in agreement with findings from SEM and optical micrography analysis, the rubbery domains were assumed to be located in interfibrillar regions. Thus the crystallinity of the iPP phase, X_c(iPP), was considered and not that of the blend.

Plots of L as a function of T_c for the neat iPP, L(iPP), and for the iPP crystallized from iPP/EPR blends, L(iPP/EPR), for all the compositions investigated, are given in Fig. 13. As shown, as expected, both L(iPP) and L(iPP/EPR) increase with increasing T_c.

For a given T_c, L is affected by blend composition and/or EPR molecular structure and composition only for the highest T_c (145 °C) investigated. In fact, at comparatively low and intermediate crystallization temperatures, L values shown by the neat iPP and iPP crystallized from its blends with EPR copolymers are within experimental error (± 0.5 nm) with no dependence on EPR content (wt/wt) and its molecular features (see Fig. 13). By increasing T_c up to 145 °C in the case of blends containing 20% (wt/wt) EPR rubbery phase, L values higher and lower than that shown by the plain iPP are exhibited by samples with EPR4 and EPR2 copolymers, respectively (see Fig. 13b).

Plots of L_c(iPP) and L_c(iPP/EPR) against blend composition result, for all the crystallization temperatures explored, in straight lines having negative slopes (see Figs 14–17). It should be pointed out that:

(i) the L_c(iPP/EPR) values are determined by blend composition irrespective of EPR molecular structure

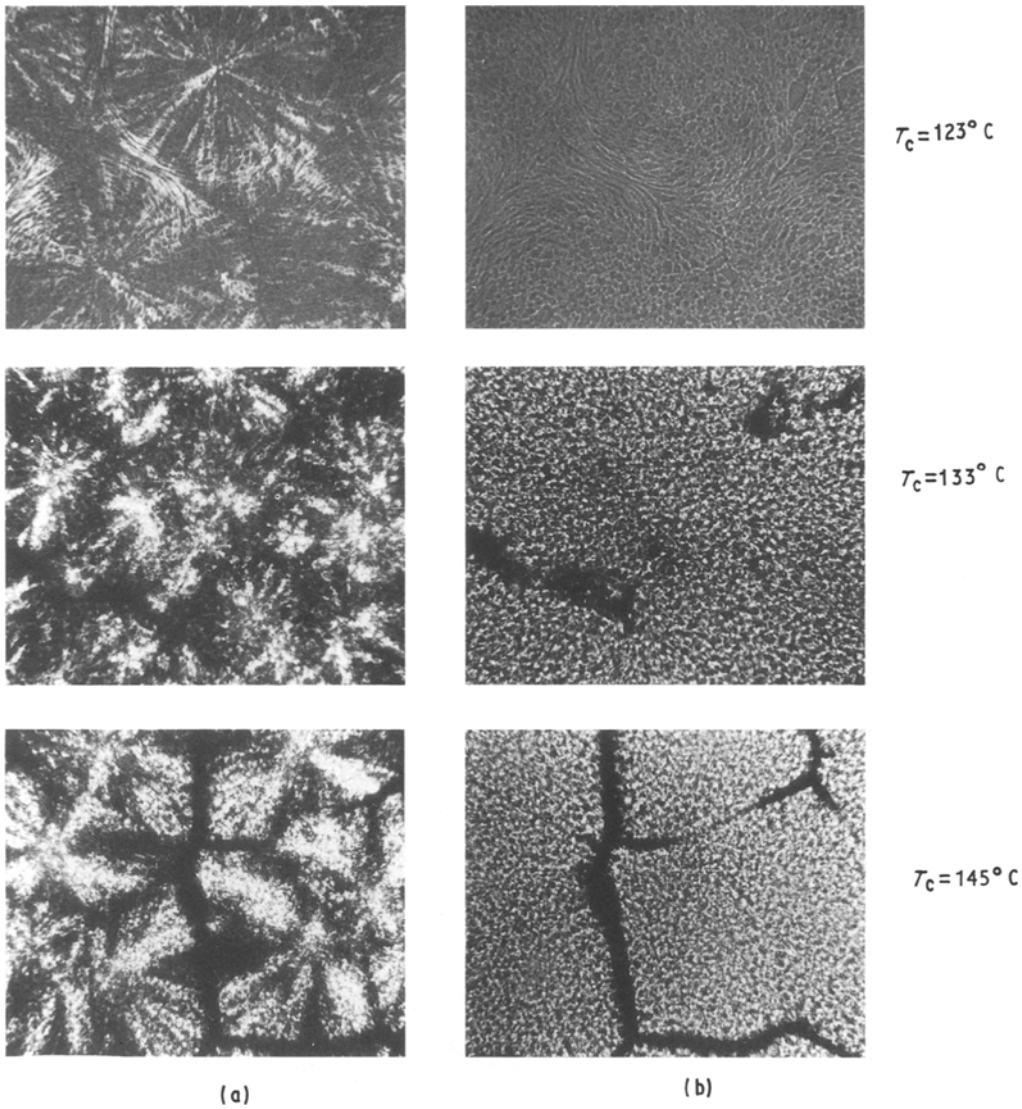

Figure 8 Optical micrographs taken at (a) crossed and (b) parallel polars of iPP/EPR3 (80/20). × 25.2.

and composition, and decrease with increasing copolymer content;

(ii) the slope of the straight lines decreases with increasing T_c (see Table VI).

Thus when iPP crystallizes from its blends in the presence of EPR copolymers, lamellar crystals are formed whose thickness, measured along a direction that is almost coincident with the chain axis, becomes lower than that of plain iPP as the EPR content and crystallization temperature increase.

Plots of L_a of the neat iPP, L_a(iPP) and iPP crystallized from its blends with EPR copolymers, L_a(iPP/EPR), as a function of blend composition result, for all crystallization temperatures explored, in straight lines with, as expected, a positive slope (see Figs 14–17).

Note that, in agreement with previous findings for L_c(iPP/EPR) values:

(i) L_a(iPP/EPR) values are determined by blend composition irrespective of EPR molecular structure and composition, and increase with increasing copolymer content;

(ii) the slope of the straight lines increases with increasing T_c (see Table VI).

Thus when iPP crystallizes from its blends in the presence of EPR copolymers, the phase structure is characterized by interlamellar amorphous layers whose thickness increases with increasing EPR content in the blend.

The finding that, for a given crystallization temperature, L_a(iPP/EPR) and L_c(iPP/EPR) increase and decrease, respectively, with increasing copolymer content, can be accounted for by assuming that during the iPP crystallization process, EPR molecules with low molecular mass are able to diffuse into the iPP interlamellar amorphous layer, probably forming domains more or less interconnected with the iPP amorphous phase. This will cause an increase in the interlamellar thickness. Owing to the development of this phase structure, apparently the crystals cannot grow freely as in the case of neat iPP. This will explain at least in part, the decreasing trend observed in L_c(iPP/EPR) with the rubber content.

3.5. Equilibrium melting temperatures and surface free energy of folding

The equilibrium melting temperatures of the neat iPP, T_m(iPP), and iPP crystallized in the presence of the

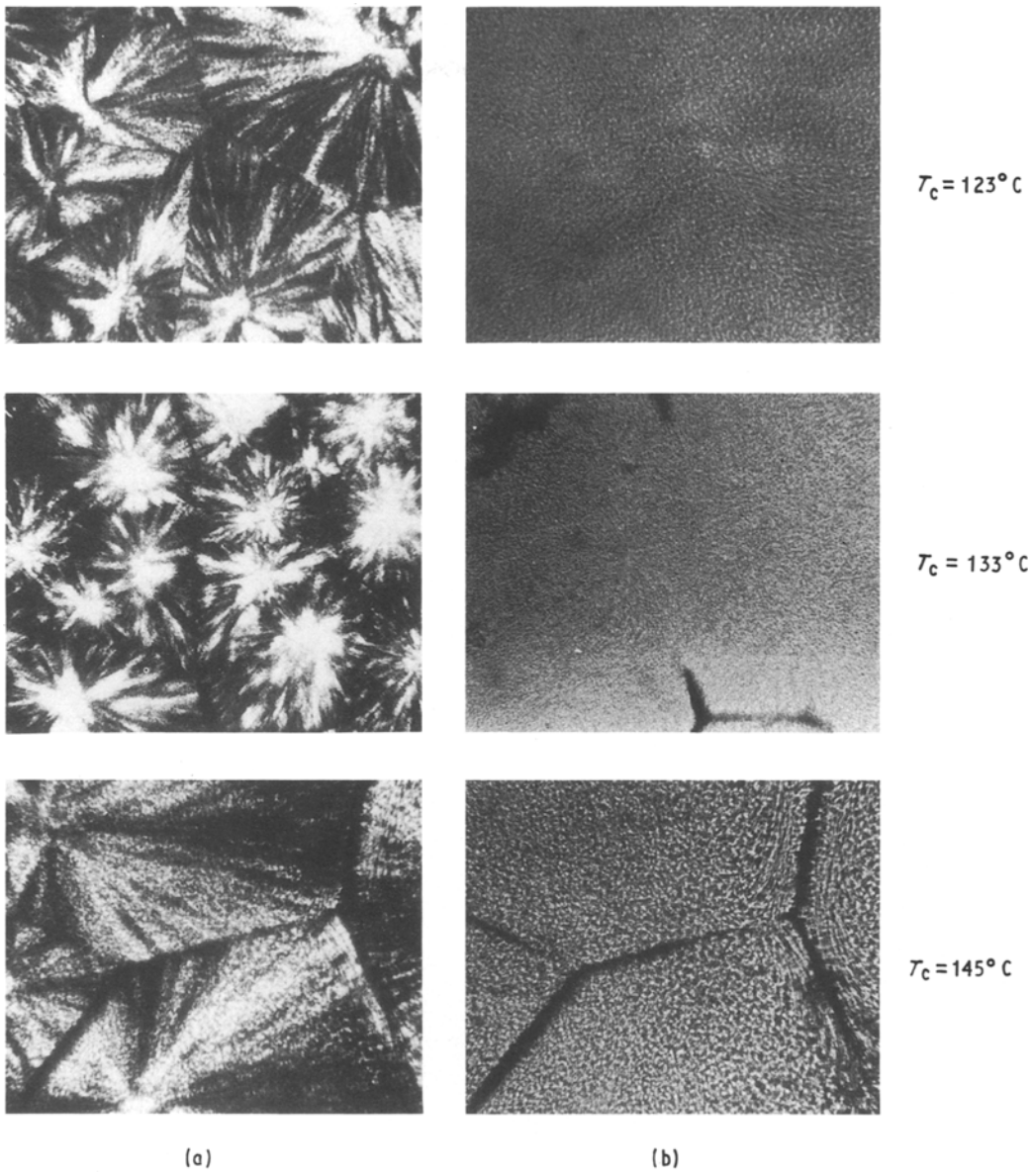

Figure 9 Optical micrographs taken at (a) crossed and (b) parallel polars of iPP/EPR4 (80/20). × 25.2.

TABLE V Range of EPR particle size developed for T_c = 133 and 145 °C, together with the EPR molecular characteristics

Sample		Range of EPR particle size (μm)		EPR Mooney viscosity, ML (1 + 4)	EPR C_3 content (% wt/wt)	EPR M_w/M_n
		T_c = 133 °C	T_c = 145 °C			
iPP/EPR1	90/10	0.5–1.5	0.5–1.5	25	27	3.5
iPP/EPR1	80/20	0.5–2.5	0.5–2.5			
iPP/EPR2	90/10	1–3	1–3	67	28	3.5
iPP/EPR2	80/20	1–4	1–4			
iPP/EPR3	90/10	2–4	2–4	80	43	5.0
iPP/EPR3	80/20	2–4	2–4			
iPP/EPR4	80/20	0.3–1	0.3–1	55	58	3.5

EPR copolymers, T_m(iPP/EPR), were determined from [11]

$$T'_m = T_m(1 - 2\sigma_e/\Delta H_f L_c) \quad (4)$$

where T'_m is the apparent melting temperature, T_m the equilibrium melting temperature, ΔH_f [6] the enthalpy of fusion of 100% crystalline iPP, L_c the lamellar crystal thickness. According to Equation 4, from the straight lines obtained by plotting T'_m against $1/L_c$, T_m and σ_e can be determined from the intercept and slope, respectively. As shown in Fig. 18 for all samples and blend compositions investigated, this equation fits the experimental data quite well.

The T_m and σ_e values determined by this method are plotted for each sample as a function of blend composition in Figs 19 and 20, respectively. Note that:

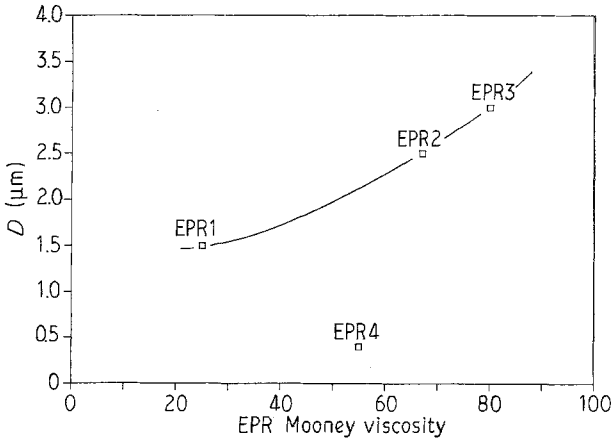

Figure 10 Plot of the EPR number average particle size versus EPR Mooney viscosity.

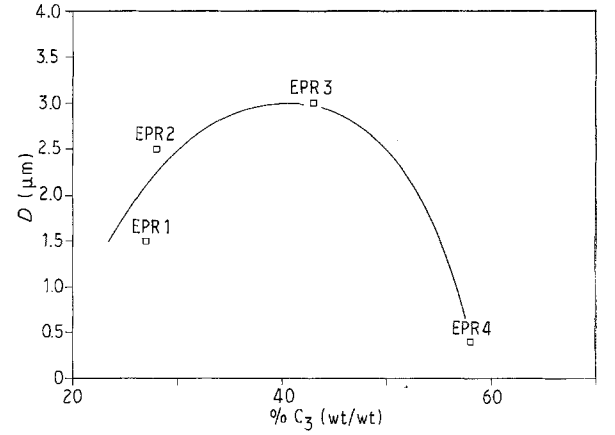

Figure 11 Plot of the EPR number-average particle size versus EPR propylene content.

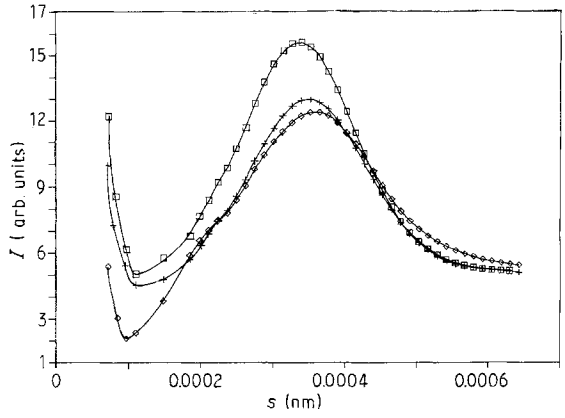

Figure 12 Typical desmeared SAXS patterns of (□) neat iPP, (+) iPP/EPR (90/10), and (◇) iPP/EPR (80/20).

(i) the values T_m(iPP) = 468 K and surface free energy of iPP, σ_e(iPP) = 133 erg cm^{-2}, agree with the values reported in literature [6],

(ii) both T_m(iPP/EPR) and the surface free energy of iPP crystallized from its blends with EPR copolymers, σ_e(iPP/EPR), are determined by the overall blend composition, almost irrespective of EPR molecular structure and composition; a slight and noticeable decrease in T_m(iPP/EPR) and σ_e(iPP/EPR)

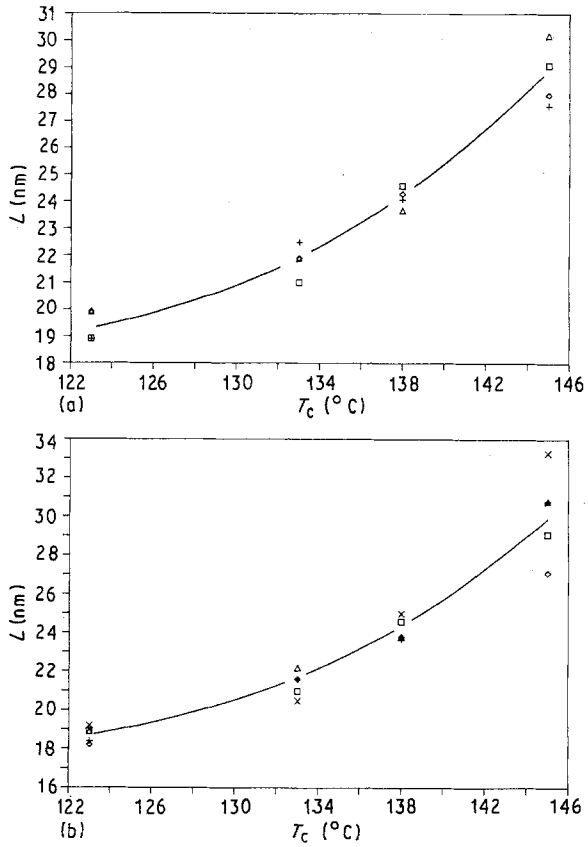

Figure 13 Plots of the long spacing, L, versus T_c for the neat iPP and for the iPP crystallized from: (a) 90/10 iPP/EPR blends, (b) 80/20 iPP/EPR blends.

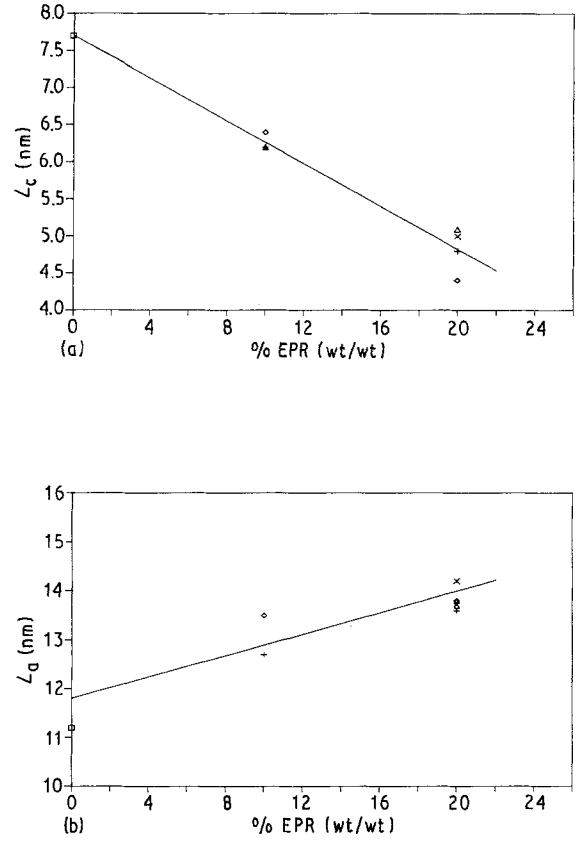

Figure 14 Plots of (a) crystalline lamella thickness, L_c, and (b) interlamellar amorphous layer, L_a, of iPP phase as a function of % EPR (wt/wt) at T_c = 123 °C; (□) iPP, (+) EPR1, (◇) EPR2, (△) EPR3, (×) EPR4.

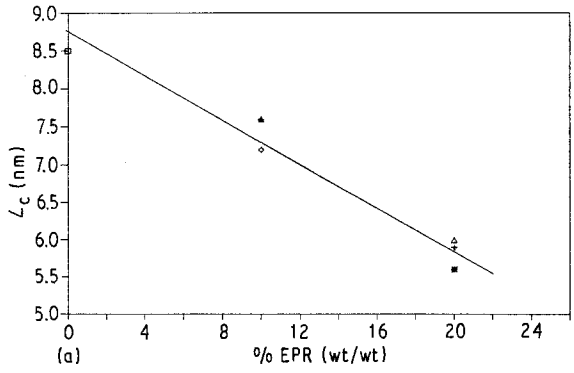

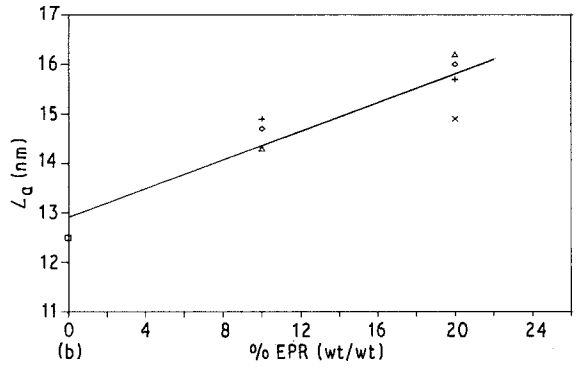

Figure 15 Plots of crystalline lamella thickness, L_c, and interlamellar amorphous layer, L_a, of iPP phase as a function of % EPR (wt/wt) at $T_c = 133\,°C$; (□) iPP, (+) EPR1, (◇) EPR2, (△) EPR3, (×) EPR4.

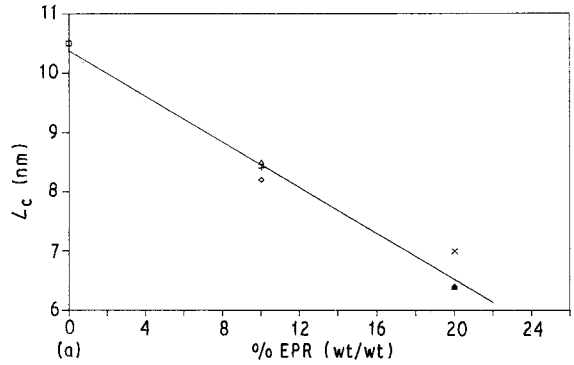

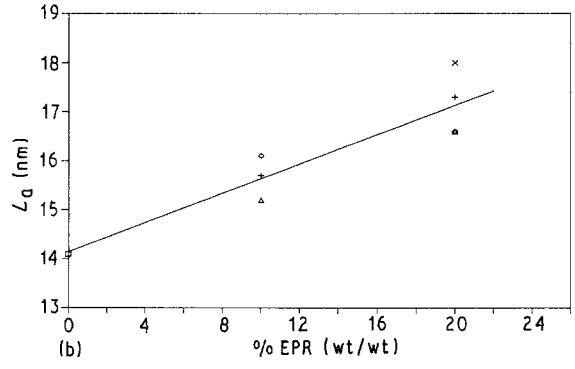

Figure 16 Plots of crystalline lamella thickness, L_c, and interlamellar amorphous layer, L_a, of iPP phase as a function of % EPR (wt/wt) at $T_c = 138\,°C$; (□) iPP, (+) EPR1, (◇) EPR2, (△) EPR3, (×) EPR4.

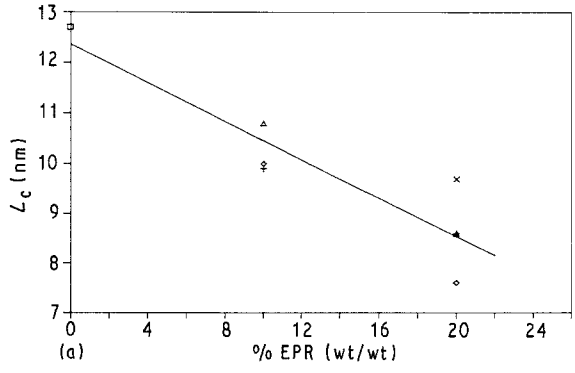

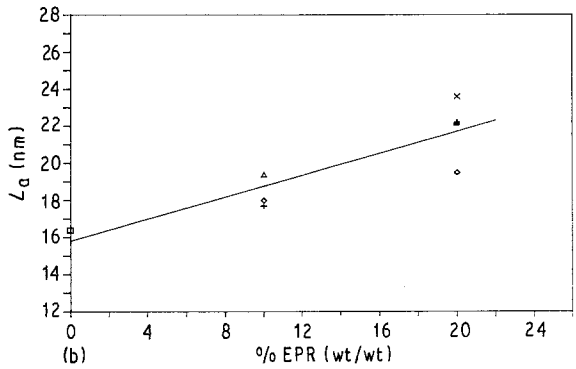

Figure 17 Plots of crystalline lamella thickness, L_c, and interlamellar amorphous layer, L_a, of iPP phase as a function of % EPR (wt/wt) at $T_c = 145\,°C$; (□) iPP, (+) EPR1, (◇) EPR2, (△) EPR3, (×) EPR4.

TABLE VI Slopes of the straight lines obtained by plotting for each explored T_c (A) L_c values against EPR content (wt/wt), (B) L_a values against EPR content (wt/wt)

T_c (°C)	A	B
123	− 1.44	1.10
133	− 1.46	1.44
138	− 1.93	1.50
145	− 2.02	2.96

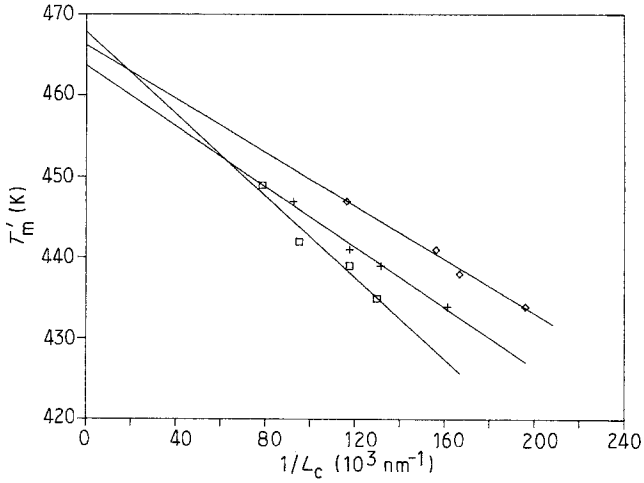

Figure 18 Typical plot of the observed melting temperatures, T'_m, as a function of reciprocal of the lamella crystal thickness, $1/L_c$; (□) iPP (100), (+) iPP/EPR3 (90/10), (◇) iPP/EPR3 (80/20).

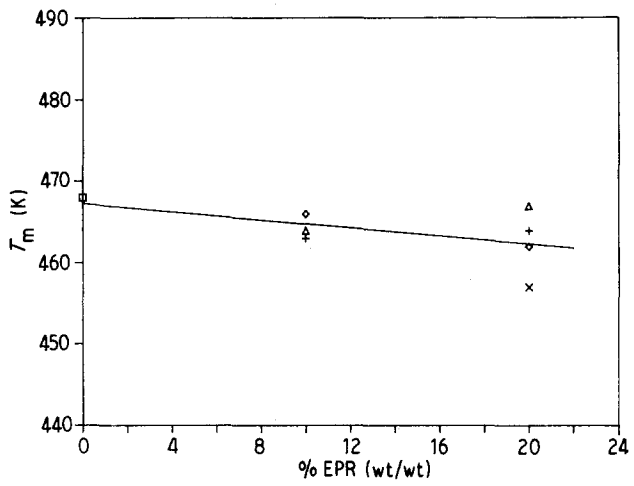

Figure 19 Plot of equilibrium melting temperatures, T_m, of iPP phase as a function of % EPR (wt/wt); (□) iPP, (+) EPR1, (◇) EPR2, (△) EPR3, (×) EPR4.

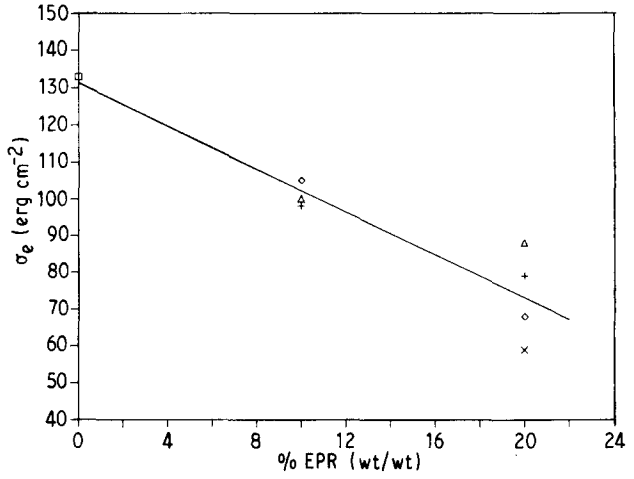

Figure 20 Plot of free energy of folding, σ_e, of iPP phase as a function of % EPR (wt/wt); (□) iPP, (+) EPR1, (◇) EPR2, (△) EPR3, (×) EPR4.

values with increasing EPR content being found, respectively.

The observed depression in T_m(iPP/EPR) values was ascribed to kinetics and morphological effect rather than to a thermodynamic effect due to the fact that iPP and EPR are incompatible in the melt.

The depression observed in σ_e(iPP/EPR) values indicates that the iPP crystals, grown in the presence of EPR phase, have a less regular surface. Such a finding can be accounted for by assuming that the iPP crystal surface is perturbed by the diffusion of molecules of EPR with low molecular mass into iPP interlamellar amorphous layers.

4. Conclusion

A study of the influence of molecular structures of EPR copolymers and composition on phase morphology and structure developed in samples of iPP/EPR blends isothermally crystallized has been reported.

The molecular structure and composition of the EPR rubbery phase play the predominant role in determining the mode and state of dispersion of the minor component. It was found, in fact, that the dispersion coarseness of the EPR spherical-shaped domains, up to a propylene content along the copolymer chain of 43% (wt/wt), is mainly determined by the EPR molecular mass, the particle size decreasing with decreasing melt-phase viscosity ratio value, in agreement with the results obtained by studying injection-moulded samples of the same iPP/EPR blends [1]. On the other hand, on increasing the propylene content further, such a parameter becomes the main factor in determining EPR particle size, the lowest dispersion coarseness of the rubbery component being found.

The EPR molecular mass results in a critical parameter, together with the overall blend composition, and also in determining the neatness and regularity of iPP spherulite texture, which appear less neat and regular with increasing copolymer content and its molecular mass.

It is, moreover, interesting to note that the crystallization process of iPP from its blends with EPR copolymers is influenced by the presence of the rubbery phase, with no regular dependence on its molecular structure and composition. The microscopic observations performed revealed that, for a given crystallization temperature, all the EPR copolymers have a very poor activity as iPP nucleating agents, contrary to the findings of Martuscelli *et al.* [12] while studying other iPP/EPR blends. Such a disagreement is explained by the fact that, in the EPR copolymers used in this work, because of the different polymerization procedure followed, a reduced number of heterogeneities (particles of impurities and/or additive) are present. Thus in such copolymers the foreign nuclei, which can migrate towards the iPP phase and induce nucleation, are missing.

It was also found that for a given crystallization temperature, the thickness of the crystalline lamella, L_c of iPP crystallized from its blends decreases, whereas the thickness of the amorphous interlamellar layer, L_a, increases. It is noted that for a given T_c, both L_c and L_a are strictly related to the overall blend composition, L_c decreasing and L_a increasing with increasing EPR content in the blend. In order to explain these results, we assumed that EPR molecules with low molecular masses, because of their higher mobility, diffuse into the iPP interlamellar amorphous layer where they may form domains more or less interconnected with the amorphous iPP phase, thus increasing its thickness and hindering the iPP crystals growth.

Other thermodynamic parameters of iPP lamellar crystals seem to be influenced by the presence of the EPR phase. In fact the equilibrium melting temperature, T_m, of iPP crystals is slightly lowered while the surface free energy of folding, σ_e, was found to be strongly depressed. Taking into account that iPP and EPR are incompatible in the melt, the observed depression in T_m of iPP crystals can be ascribed to kinetics and a morphological effect, rather than to a thermodynamic effect. However, in a previous work dealing with iPP/EPR blends, Martuscelli *et al.* [12] found an increase in T_m of iPP crystallized in the presence of EPR phase. To explain such a result, an

hypothesis of a selective dissolution of a certain amount of the more defective iPP molecules into EPR was formulated. The failure of such an hypothesis in our results is due to the fact that the iPP used in this work, obtained by a different catalyst system (very high yield Ziegler–Natta $MgCl_2$ supported catalysts), has a higher isotacticity index; i.e. a lower amount of configurational irregularities distributed along the macromolecules. Consequently, the EPR phase does not dissolve any appreciable amount of iPP molecules.

The finding that the iPP crystals, grown in the presence of EPR phase, have a less regular surface may be accounted for by assuming that the iPP crystal surface is perturbed by the diffusion of low EPR molecular masses into the iPP interlamellar amorphous layer.

Acknowledgement

This work was partly supported by Progetto Finalizzato Chimica fine II of C.N.R. Sottoprogetto Chimica e Tecnologia dei Polimeri.

References

1. L. D'ORAZIO, C. MANCARELLA and E. MARTUSCELLI, *Polymer*, in press.
2. M. L. ADDONIZIO, L. D'ORAZIO, C. MANCARELLA and E. MARTUSCELLI, *J. Mater. Sci.* **24** (1989) 2939.
3. G. I. TAYLOR, *Proc. R. Soc. Lond. A* **146** (1934) 501.
4. S. TOMOTIKA, *ibid.* **150** (1935) 322.
5. *Idem., ibid.* **153** (1936) 308.
6. S. BRANDRUP and E. M. IMMERGUT, "Polymer Handbook", Vol. 5 (Interscience, New York, 1975) p. 24.
7. O. J. GLATTER, *Appl. Crystallogr.* **7** (1974) 147.
8. L. E. ALEXANDER, "X-ray Diffraction in Polymer Science" (Wiley, New York, 1969).
9. E. MARTUSCELLI, *Polym. Engng Sci.* **24**(8) (1984) 563.
10. *Idem., ibid.* **24**(15) 1155.
11. J. D. HOFFMAN, *SPE Trans.* **4** (1964) 315.
12. E. MARTUSCELLI, C. SILVESTRE and G. ABATE, *Polymer* **23** (1982) 229.

Received 2 October
and accepted 19 November 1990